Journal of Interdisciplinary Mathematics
ISSN: 0972-0502 (Print), ISSN: 2169-012X (Online)
Vol. 29 (2026), No. 4, pp. 861–873
DOI : 10.47974/JIM-2324

Numerical simulation of Korteweg-de Vries equation with moving boundaries

Nurbol Koshkarbayev
Institute of Mathematics and Mathematical Modeling
125 Pushkin str.
050010 Almaty
Kazakhstan

Abstract

We consider the Korteweg–de Vries equation posed on a spatial interval whose endpoints evolve in time. The spatial discretization is carried out by a Galerkin finite-element formulation based on B-spline basis functions, whereas temporal integration uses the Crank–Nicolson scheme. Benchmark tests confirm that the proposed algorithm attains high accuracy while remaining computationally efficient. The results illustrate that the method robustly captures wave propagation in domains with moving boundaries.

Subject Classification (2020): *35Q53, 35R37, 65N22, 65M60.*

Keywords: *Korteweg–de vries equation, B-spline finite elements, Time-dependent (moving) boundaries, Crank–Nicolson time stepping, Numerical simulation.*

1. Introduction

1.1 *Modeling equation*

We begin with the classical Korteweg–de Vries (KdV) equation [1] written in dimensional variables. It describes one–directional (to the right) propagation of weakly nonlinear, weakly dispersive surface waves:

$$\frac{\partial \eta}{\partial t} + c\left(1 + \frac{3h}{2}\eta\right)\frac{\partial \eta}{\partial x} + \frac{ch^2}{6}\frac{\partial^3 \eta}{\partial x^3} = 0, \tag{1.1}$$

$\eta(x, t)$ represents the deviation of the free water surface from its undisturbed position, h is the uniform depth of the still water, and the linear gravity wave speed is given by $c = \sqrt{hg}$, where g denotes the acceleration due to gravity.

After nondimensionalization and a change of variables, the model can be recast in the compact form

ORCID-ID: **0000-0003-2563-0693**

E-mail: **koshkarbaev.nurbol@gmail.com**

$$\frac{\partial v}{\partial t}+\varepsilon v\frac{\partial v}{\partial y}+\mu\frac{\partial^3 v}{\partial y^3}=0,\quad y\in(a,b),\quad t>0,$$

with ε and μ and fixed endpoints $a<b$ of the spatial interval.

The Korteweg–de Vries equation is a prototypical nonlinear dispersive evolution and arises in many branches of physics and engineering. Examples include ion–acoustic solitons in plasma physics and long internal or surface waves in geophysical fluid dynamics (e.g., [2, 3]). Its relevance also extends to cluster physics, superdeformed nuclei, nuclear fission, thin–film flows, radar signal analysis, and other areas (see [4, 5]).

1.2 *Formulation of main problem*

Let

$$\widehat{\Omega}=\{(y,\tau)\in\mathbb{R}^2;\ y\in(a(\tau),b(\tau)),\qquad \tau\in(0,T)\}$$

represent a time-dependent (noncylindrical) space–time domain with a moving lateral boundary indicated by

$$\hat{E}=\bigcup_{0<\tau<T}\Gamma_\tau\times\{\tau\},$$

where $Q_\tau=\{y\in\mathbb{R};\ a(\tau)<y<b(\tau),\ 0<\tau<T\}$ and Γ_τ denotes the boundary of Q_τ. We study the nonlinear initial–boundary value problem for the KdV equation in this non-cylindrical domain:

$$\begin{cases}\dfrac{\partial v}{\partial \tau}+v\dfrac{\partial v}{\partial y}+\dfrac{\partial^3 v}{\partial y^3}=0, & (y,\tau)\in\widehat{\Omega},\\ v(a(\tau),\tau)=v(b(\tau),\tau)=0, & \\ \dfrac{\partial v}{\partial y}(b(\tau),\tau)=0, & \tau\in[0,T),\\ v(y,0)=v_0(y), & y\in Q_0.\end{cases}\tag{1.2}$$

The well-posedness of IBVPs for the classical constant-coefficient KdV equation posed on cylindrical domains has been established by numerous authors, including Bubnov [6], Khablov [7], Bona, Sun, and Zhang [8], Boutet de Monvel and Shepelsky [9], Faminskii [10, 11], and Larkin [12, 13], among others. Their analyses cover a wide range of function spaces and boundary conditions. In contrast, the present work treats the case where the boundaries move in time, introducing additional analytical and numerical challenges.

When these equations are used to model wave phenomena and a numerical method is required, it is common to restrict attention to a finite spatial interval (cf. [8, 14, 15] for a KdV example). In real settings, however, the wave-supporting region itself can vary with time. This time dependence of the domain enhances both the modeling realism and the analytical challenge of the problem.

In [16], Doronin and Larkin investigated the problem described in (1.2) and demonstrated both the existence and uniqueness of strong global solutions, along with the exponential decay of global solutions. One reason for continuing research on KdV equations is their potential applications in numerical simulations. For instance, it could be intriguing to examine how the trajectory of a family of solitons behaves when tracked effectively within a domain that has moving boundaries.

In this study, we utilize an approximate solution for the problem described in equation (1.2). Additionally, we clarify that the effect of boundaries is explained using numerical examples. Our main contribution is providing numerical results for the problem (1.2). Based on what we know, this is the first time such an effort has been undertaken for the KdV equation in a non-cylindrical domains.

1.3 *Reduction to a problem with fixed boundaries*

Let us define the function $p(\tau)$ for all $\tau \in (0,T)$ by $p(\tau) = b(\tau) - a(\tau)$. Here, the functions $a(\tau)$ and $b(\tau)$ are in $C^2(0,T)$ and are constrained for all $\tau \in (0,T)$ such that $a(\tau)$ is non-increasing, $b(\tau)$ is non-decreasing, and the inequality $a(\tau) < b(\tau)$ holds.

To convert the moving spatial interval into a fixed one, we introduce the change of variables

$$x = \frac{y-a(\tau)}{p(\tau)}, \qquad (y,\tau) \in \widehat{\Omega},$$

so that $x \in (0,1)$ whenever $y \in (a(\tau), b(\tau))$. This defines a mapping

$$\begin{aligned} &\mathcal{J}: \widehat{\Omega} \to \Omega = (0,1) \times (0,T), \\ &(y,\tau) \to (x,t) = \left(\frac{y-a(t)}{p(t)}, t\right). \end{aligned} \tag{1.3}$$

Transformation $\mathcal{J}$ is differentiable twice continuously and its inverse $\mathcal{J}^{-1}$ is also differentiable twice continuously. The technique of converting a domain with a moving boundary into one with a fixed boundary has been utilized in previous studies (see [17, 18]).

Define

$$u(x,t) = v(a(t) + p(t)x, t).$$

Applying the above change of variables to problem (1.2) produces an equivalent mixed initial-boundary-value problem on a time-independent cylinder Ω:

$$\begin{cases} \frac{\partial u}{\partial t} - \alpha(x,t)\frac{\partial u}{\partial x} + \beta_1(t) u \frac{\partial u}{\partial x} + \beta_2(t)\frac{\partial^3 u}{\partial x^3} = 0, & (x,t) \in \Omega, \\ u(0,t) = u(1,t) = 0, & \\ \frac{\partial u}{\partial x}(1,t) = 0, & t \in (0,T), \\ u(x,0) = u_0(x), & x \in (0,1), \end{cases} \tag{1.4}$$

where $\Omega = (0,1) \times (0,T)$ is a cylindrical domain and

$$\alpha(x,t) = \frac{a'(t) + x p'(t)}{p(t)}, \qquad \beta_1(t) = \frac{1}{p(t)}, \qquad \beta_2(t) = \frac{1}{p^3(t)}. \tag{1.5}$$

2. Approximation scheme

In this section, we compute numerical approximations of the solution. Two discretization strategies are employed: Galerkin finite elements (FEM) together with a finite difference (FDM) time/space discretization. We also carried out numerical experiments to assess the impact of moving boundaries on the Korteweg–de Vries dynamics.

To simplify the implementation of FEM, we work with the transformed formulation (1.4) posed on the fixed rectangle $\Omega = (0,1) \times (0,T)$, instead of the original problem (1.2) with time-dependent spatial limits.

2.1 *Variational approach*

Multiplying Equation (1.4) by $\omega \in H_0^1(0,1)$, integrating over $(0,1)$ and then applying integration by parts, leads to the following variational formulation:

$$\begin{aligned} \int_0^1 \frac{\partial u}{\partial t}\omega dx \quad &- \int_0^1 \alpha(x,t)\frac{\partial u}{\partial x}\omega dx + \beta_1(t)\int_0^1 u\frac{\partial u}{\partial x}\omega dx \\ &+\beta_2(t)\int_0^1 \frac{\partial^3 u}{\partial x^3}\omega dx = 0, \quad \forall\omega \in H_0^1(0,1), \end{aligned} \tag{2.1}$$

where certain terms have been substituted for ease of calculation.

2.2 *Galerkin approach and approximation*

Let $V = H_0^1(\Omega)$ and choose a finite-dimensional subspace V_m represents the subspace spanned by

$$u^h(x,t) = \sum_{i=1}^m c_i(t)\varphi_i(x), \qquad \varphi_i(x) \in V_m. \tag{2.2}$$

Inserting the assumed form of the solution into the weak formulation (2.1) and testing with $\omega = \varphi_j(x) \in V_m$, we obtain

$$\begin{aligned} &\sum_{i=1}^m c_{i'}(t)\int_0^1 \varphi_i\varphi_j dx + \beta_1(t)\sum_{i=1}^m \sum_{k=1}^m c_i(t)c_k(t)\int_0^1 \varphi_i\frac{\partial\varphi_k}{\partial x}\varphi_j dx \\ &-\sum_{i=1}^m c_i(t)\int_0^1 \alpha(x,t)\frac{\partial\varphi_i}{\partial x}\varphi_j dx - \beta_2(t)\sum_{i=1}^m c_i(t)\int_0^1 \frac{\partial^2\varphi_i}{\partial x^2}\frac{\partial\varphi_j}{\partial x}dx = 0, \end{aligned} \tag{2.3}$$

for each $j = 1,\dots,m$. Introduce the coefficient arrays

$$A_{ij} = \int_0^1 \varphi_i\varphi_j dx, \quad B_{ij}(t) = \int_0^1 \alpha(x,t)\frac{\partial\varphi_i}{\partial x}\varphi_j dx, \; D_{ij} = \int_0^1 \frac{\partial^2\varphi_i}{\partial x^2}\frac{\partial\varphi_j}{\partial x}dx,$$

and the third-order tensor

$$C_{ikj} = \int_0^1 \varphi_i\frac{\partial\varphi_k}{\partial x}\varphi_j dx.$$

Then (2.3) takes the compact vector form

$$\begin{cases} Ac'(t) + Gc(t) + \beta_1(t)Cc^2(t) = 0, \\ c(0) = c_0, \end{cases} \tag{2.4}$$

where $G = -B(t) - \beta_2(t)D$ and $c(t) = (c_1(t),\dots,c_m(t))$.

2.3 *Finite difference scheme*

Direct integration of the nonlinear ODE system (2.4) is inconvenient when the coefficient matrices depend on both x and t. We therefore discretize in time using an implicit second-order scheme of Crank–Nicolson type (cf. [19]).

Let $t_n = n\Delta t, n = 0,1,2,\dots,N,$ with $\Delta t = T/N,$ and denote by

$$c^n(t) \approx c(t_n) \in \mathbb{R}^m$$

the discrete solution vector. (For any matrix or tensor-valued quantity $W(t)$, we write $W^n = W(t_n)$). To handle the quadratic nonlinearity involving the third-order tensor C_{ikj}, we linearize it around the known value c^n. Define, for each $k = 1, \ldots, m$, the matrix

$$C_{ij}^{(k)} = C_{ikj} c_k(t), \qquad 1 \leq i, j \leq m.$$

Then the nonlinear term in (2.3)-(2.4) can be expressed schematically as

$$\hat{C}_{ij}^n c_i(t) := \sum_{k=1}^m (C_{ikj} c_k(t)) c_i^n(t).$$

and, under Crank–Nicolson averaging, we approximate

$$\hat{C}_{ij}^n c_i^n = \frac{1}{2} \hat{C}_{ij}^n (c_i^{n+1} + c_i^n). \tag{2.5}$$

Using the finite difference

$$c'_i(t_n) = \frac{c_i^{n+1} - c_i^n}{\Delta t},$$

substituting $t = t_n$ into (2.4), and applying (2.5), we obtain for each $j = 1, \ldots, m$:

$$A_{ij} \left(\frac{c_i^{n+1} - c_i^n}{\Delta t}\right) + (G_{ij}^n + \beta_1(t) \hat{C}_{ij}^n) \left(\frac{c_i^{n+1} + c_i^n}{2}\right) = 0. \tag{2.6}$$

Multiplying (2.3) by Δt and regrouping terms yields the linear system

$$\left(A_{ij} + \frac{\Delta t}{2} J_{ij}^n\right) c_i^{n+1} = \left(A_{ij} - \frac{\Delta t}{2} J_{ij}^n\right) c_i^n, \text{ for } n = 0,1,2,.., \tag{2.7}$$

where $J_{ij}^n := G_{ij}^n + \beta_1(t) \hat{C}_{ij}^n$.

This iterative scheme produces c^{n+1} by solving an $m \times m$ linear system at each time level. The nonlinearity enters only through the updated matrix J^n, which is recomputed at every step using the known vector c^n.

2.4 *Finite element method based on Galerkin principles*

To assemble the matrices in the linear system (2.7), we introduce a finite element basis $\{\varphi_i\}_{i=1}^m \in V_m$. In FEM, one typically chooses piecewise polynomial functions on Q that vanish on ∂Q. In our case, because the matrix D_{ij} in (2.3) involves second and third derivatives, we adopt cubic B-splines as basis functions for V_m,

Let the nodes be uniformly spaced:

$$0 = x_1 < \ldots < x_m = 1, \qquad h = x_{i+1} - x_i.$$

The (cardinal) cubic B-spline $B^{(3)}(x)$ centered at x_i is supported on $[x_{i-2}, x_{i+2}]$ nd can be written (for $i = 1, \ldots, m$) as

$$B_l^{(3)}(x) = \begin{cases} \frac{(x-x_{l-2})^3}{4h^3}, & \text{for} \quad x \in [x_{l-2}, x_{l-1}), \\ \frac{1}{4} + \frac{3(x-x_{l-1})}{4h} + \frac{3(x-x_{l-1})^2}{4h^2} - \frac{3(x-x_{l-1})^3}{4h^3}, & \text{for} \quad x \in [x_{l-1}, x_l), \\ \frac{1}{4} + \frac{3(x_{l+1}-x)}{4h} + \frac{3(x_{l+1}-x)^2}{4h^2} - \frac{3(x_{l+1}-x)^3}{4h^3}, & \text{for} \quad x \in [x_l, x_{l+1}), \\ \frac{(x_{l+2}-x)^3}{4h^3}, & \text{for} \quad x \in [x_{l+1}, x_{l+2}), \\ 0, & \text{otherwise}, \end{cases}$$

One checks that

$$B_l^{(3)}(x_l) = 1, \qquad B_l^{(3)}(x_{l-1}) = B_l^{(3)}(x_{l+1}) = \frac{1}{4}$$

and $B_i^{(3)}$ vanishes at all other nodes. We intend to use $B_1^{(3)}, B_2^{(3)}, \ldots, B_m^{(3)}$ as the raw building blocks, but the first two and last two splines do not automatically satisfy the homogeneous boundary conditions. Therefore, we define the actual basis $\{\varphi_i\}$ as

$$\varphi_i(x) = \begin{cases} 0, & i = 1 \text{ or } i = m, \\ B_0^{(3)}(x) - \frac{1}{2}B_1^{(3)}(x) + B_2^{(3)}(x), & i = 2, \\ B_{m-1}^{(3)}(x) - \frac{1}{2}B_m^{(3)}(x) + B_{m+1}^{(3)}(x), & i = m-1, \\ B_i^{(3)}(x), & 3 \le i \le m-2. \end{cases} \tag{2.8}$$

where $B_0^{(3)}(x)$ and $B_{m+1}^{(3)}$ denote the B-splines associated with the fictitious points $x_0 = x_1 - h$ and $x_{m+1} = x_m + h$, respectively. so the basis satisfies the required boundary conditions.

With these basis functions, all the entries in (2.3) and hence in the matrix $(A_{ij} + \frac{\Delta t}{2} J_{ij}^n)$, of (2.7) can be computed. Each resulting matrix is heptadiagonal (seven nonzero diagonals). It is straightforward to verify that the coefficient matrix remains nonsingular at every discrete time t_n. From (2.2), the discrete solution reads

$$u^h(x,t) = \sum_{i=1}^{m} c_i(t)\varphi_i(x), \qquad \varphi_i(x) \in V_m.$$

After solving (2.7) for $c^n = (c_1^n, c_2^n, \ldots, c_m^n)^T$, we obtain the FEM approximation $u^h(x,t)$ to problem (1.4) in the subspace V_m. Since the mapping $\mathcal{J}$ introduced in (1.3) is an isomorphism, this discrete solution for the fixed domain problem (1.4) immediately yields an approximation to the original moving-boundary problem (1.2) via the inverse transformation $y = a(t) + p(t)x$.

3. Simulation results

In this section we implement and test the proposed approximation schemes. To benchmark the iterative method (2.7), we employ a manufactured forcing term $f(y,\tau)$ on the right-hand side of the original problem (1.2), rather than setting $f(y,\tau) \equiv 0$. By choosing f appropriately, we can prescribe a sufficiently smooth exact solution and thus assess the accuracy of the numerical method in the absence of established (continuous or discrete) error estimates for (1.2) or its transformed counterpart (1.4). Under the change of variables (1.3), the corresponding source term in the fixed-domain formulation is denoted by $r(x,t)$.

We then carried out a series of experiments to investigate how moving boundaries affect the Korteweg–de Vries dynamics. In particular, following the setup in [20], we consider two representative boundary motion parameters, $q = 1$ and $q = (0.022)^2$, and compare the resulting solution behaviors. This framework enables us to examine the convergence properties and quantify the influence of boundary motion on the numerical solution.

We study the nonhomogeneous initial–boundary value problem

$$\begin{cases} \frac{\partial u}{\partial t} - \alpha(x,t)\frac{\partial u}{\partial x} + \beta_1(t)u\frac{\partial u}{\partial x} + \beta_2(t)\frac{\partial^3 u}{\partial x^3} = r(x,t), & (x,t) \in \Omega, \\ u(0,t) = u(1,t) = 0, & \\ \frac{\partial u}{\partial x}(1,t) = 0, & \forall t \geqslant 0, \\ u(x,0) = x^2(x-1)^2, & 0 \le x \le 1, \end{cases} \tag{3.1}$$

posed on the fixed cylinder $\Omega = (0,1) \times (0,T)$. This formulation coincides with the transformed problem (1.4) when the forcing term vanishes, i.e., for $r(x,t) \equiv 0$.

3.1 *Numerical example 1*

Let the endpoints of the spatial interval be given by

$$a(t) = -\frac{t}{t+1}, \; b(t) = \frac{2t+1}{t+1}. \tag{3.2}$$

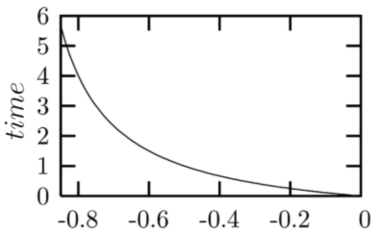

Boundary $a(t)$

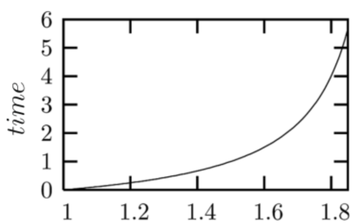

Boundary $b(t)$

As $t \to \infty$ has $a(t) \to -1$, $b(t) \to 2$ and consequently $p(t) \to 3$. Figures 1 and 2 (see below) illustrate how the endpoints $a(t)$ and $b(t)$ evolve over time. Using the definitions in (3.2), the coefficient functions in (1.4) become

$$\alpha(x,t) = \frac{a'(t) + xp'(t)}{p(t)}, \quad \beta_1(t) = \frac{1}{p(t)}, \quad \beta_2(t) = \frac{q}{p^3(t)},$$

To verify the accuracy of our iterative Crank–Nicolson scheme (2.7), we prescribe a smooth forcing term $r(x,t)$ (the transformed version of $f(y,\tau)$ under the mapping (1.3)) so that the exact solution is known. Choosing

$$r(x,t) = x^4 - 2x^3 + x^2 - (\alpha(x,t)(4x^3 - 6x^2 + 2x) - \beta_2(t)(24x - 12))(1+t) + \beta_1(t)(4x^7 - 12x^6 + 22x^5 - 10x^4 + 2x^3)(t+1)^2.$$

ensures that

$$u(x,t) = x^2(x-1)^2(t+1)$$

solves system (3.1) with the parameters defined in (3.2).

We quantify the discrepancy between the exact solution $u(x,t)$ and the numerical approximation $u^h(x,t)$ using the norm

$$E_{L^\infty(0,T,L^2(0,1))} = \max_{t_n\in[0,1]} \left(\int_0^1 |u(x,t_n) - u^h(x,t_n)|^2 dx\right)^{\frac{1}{2}}. \tag{3.3}$$

(Here $t_n = n\Delta t$, $n = 0,1,\dots,N$ and we evaluate the integral using the discrete mesh points.) Below are the errors computed for two fixed time steps Δt and different mesh sizes h, for two representative values of the parameter q.

Table 1

N	m	Error
100	10	0.002244
100	20	0.002181
100	50	0.002172
100	100	0.002171

Table 2

N	m	Error
1000	10	0.0004147
1000	20	0.0002393
1000	50	0.0002289
1000	100	0.0002284

Table 3

N	m	Error
100	10	0.0004905
100	20	0.0003458
100	50	0.0003297
100	100	0.0003296

Table 4

N	m	Error
1000	10	0.0002765
1000	20	0.0000542
1000	50	0.0000331
1000	100	0.0000329

The errors for $q = 1$ are reported in Tables 1 and 2, while those for $q = (0.022)^2$ are given in Tables 3 and 4. In all experiments, 100 iterations were used for $\Delta t = 0.01$ and 1000 iterations for $\Delta t = 0.001$ in the iterative scheme (2.7).

From Tables 1–4 we observe algebraic convergence with respect to the spatial mesh size h (or the number of elements m) and the time step Δt (or the number of time levels N): the error $E_{L^\infty((0,T);L^2(0,1))}$ decreases as h and Δt are refined, as expected.

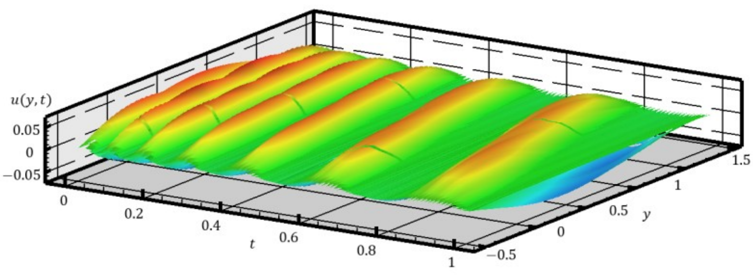

Figure 1
Numerical solution $u^h(x,t)$ corresponding to (3.1) with $q = 1$.

These results confirm that the proposed numerical method is effective. Therefore, we apply the same procedure to compute the numerical solution of (3.1) in the homogeneous case $r(x,t) \equiv 0$, which corresponds to $f \equiv 0$ in the original problem (1.2).

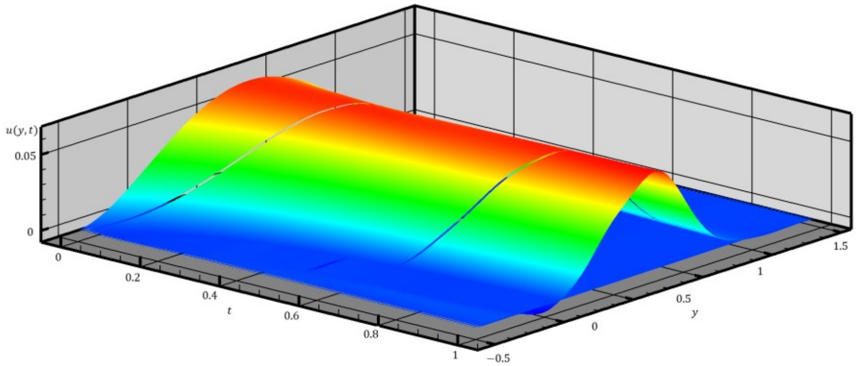

Figure 2
Numerical solution $u^h(x,t)$ corresponding to (3.1) with $q = (0.022)^2$.

Figure 1 displays the numerical solution for $q = 1$ with $f \equiv 0$, while Figure 2 shows the case $q = (0.022)^2$ and $f \equiv 0$. Both figures illustrate wave propagation in a time-dependent spatial domain; in each case, the solution amplitude diminishes as t increases.

3.2 *Numerical example 2*

Let $Q_t = (a(t), b(t))$ its moving spatial boundaries define

$$a(t) = -1 + 0.01\, e^{-t-1}, \qquad b(t) = 1 - 0.01\, e^{-t-1}. \tag{3.4}$$

The plots of the moving boundaries $a(t)$ and $b(t)$ are shown in Figure 3. Hence,

$$p(t) = b(t) - a(t) = 2 - 0.02\, e^{-(t+1)}.$$

It follows that

$$\lim_{t\to\infty} a(t) = -1, \qquad \lim_{t\to\infty} b(t) = 1, \qquad \lim_{t\to\infty} p(t) = 2.$$

The errors for $q = 1$ are listed in Tables 5 and 6; the errors for $q = (0.022)^2$ appear in Tables 7 and 8. As in Example 1, the results show a consistent reduction of the error (3.3) as the spatial and temporal grids are refined. This confirms that the numerical scheme remains effective for the second boundary configuration. Therefore, the same algorithm can be applied to solve (3.1) in the homogeneous formulation $r(x,t) \equiv 0$, and in the original formulation (1.2) this corresponds to $f(y,\tau) \equiv 0$.

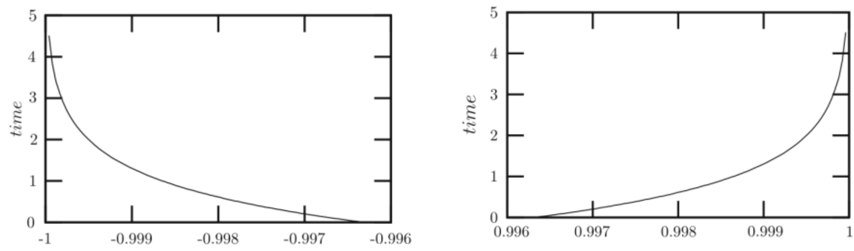

Figure 3
Time evolution of the left boundary $a(t)$ and the right boundary $b(t)$ in Numerical Example 2.

Table 5

N	m	Error
100	10	0.0002765
100	20	0.0000501
100	50	0.0000174
100	100	0.0000170

Table 6

N	m	Error
1000	10	0.0002765
1000	20	0.0000473
1000	50	0.0000045
1000	100	0.0000003

Table 7

N	m	Error
100	10	0.0003257
100	20	0.0000512
100	50	0.0000076
100	100	0.0000058

Table 8

Δt	h	Error
0.001	0.1	0.0003134
0.001	0.05	0.0000483
0.001	0.02	0.0000044
0.001	0.01	0.0000003

Figure 4 displays the numerical solution for $q = 1$ with $f \equiv 0$, and Figure 5 corresponds to $q = (0.022)^2$ with $f \equiv 0$. In both cases, the wave propagates within a time-dependent domain, and the solution amplitude diminishes as t increases.

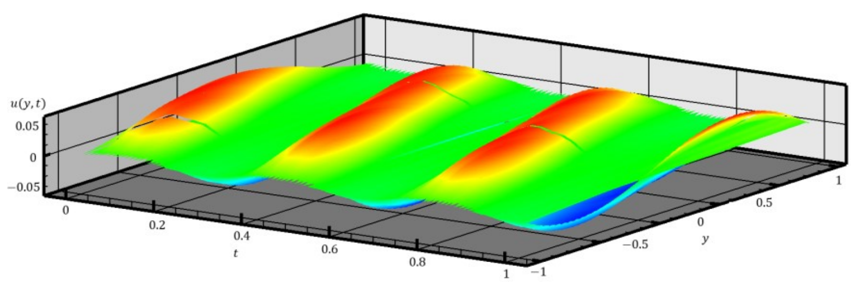

Figure 4
Numerical solution $u^h(x,t)$ corresponding to (3.1) with $q = 1$.

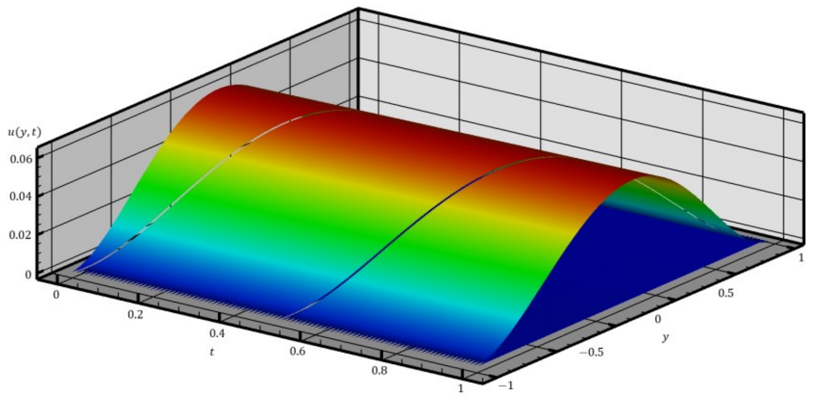

Figure 5
Numerical solution $u^h(x,t)$ corresponding to (3.1) with $q = (0.022)^2$.

Declaration of competing interest

The authors report no conflicts of interest in relation to this study.

Acknowledgments

This work was supported by the Science Committee of the Ministry of Science and Higher Education of the Republic of Kazakhstan (Grant No. AP22686595).

References

[1] D. J. Korteweg and G. de Vries, "On the change of form of long waves advancing in a rectangular canal and on a new type of long stationary waves," *Philosophical Magazine,* ser. 5, vol. 39, no. 5, pp. 422–443 (1895). doi: 10.1080/14786449508620739.

[2] A. Osborne, "The inverse scattering transform: Tools for the nonlinear Fourier analysis and filtering of ocean surface wave," *Chaos, Solitons and Fractals,* vol. 5, no. 12, pp. 2623–2637 (1995). doi: 10.1016/0960-0779(94)E0118-9.

[3] L. Ostrousky and Y. A. Stepanyants, "Do internal solitons exist in the ocean?," *Rev. Geophys.*, vol. 23, no. 3, pp. 293–310 (1989). doi: 10.1029/RG027i003p00293.

[4] L. Reatto and D. Galli, "What is ROTON?," *Int. J. Mod. Phys. B,* vol. 13, nos. 05–06, pp. 607–616 (1999). doi: 10.1142/S0217979299000497.

[5] A. Ludu and J. P. Draayer, "Nonlinear modes of liquid drops as solitary waves," *Phys. Rev. Lett.,* vol. 80, no. 10, pp. 2125–2128 (1998). doi: 10.1103/PhysRevLett.80.2125.

[6] B. A. Bubnov, “General boundary-value problems for the Korteweg–de Vries equation in a bounded domain,” *Differ. Uravn.*, vol. 15, no. 1, pp. 26–31 (1979). (in Russian). doi: https://www.mathnet.ru/eng/de3591.

[7] V. V. Khablov, “On a boundary-value problem for the Korteweg–de Vries equation in a bounded domain,” in Primenenie metodov funkcional’nogo analiza k zadacham matematicheskoi fiziki i vychislitel’noi matematiki, V. N. Vragov, Ed. Novosibirsk: Inst. Mat., Sib. Otdel., Akad. Nauk SSSR, pp. 137–141 (1979). (in Russian). MR0584772.

[8] J. L. Bona, S. M. Sun, and B.-Y. Zhang, “A nonhomogeneous boundary-value problem for the Korteweg–de Vries equation posed on a finite domain,” *Commun. Partial Differ. Equ.*, vol. 28, nos. 7–8, pp. 1391–1436 (2003). doi: 10.1081/PDE-120024373.

[9] A. Boutet de Monvel and D. Shepelsky, “Initial boundary value problem for the mKdV equation on a finite interval,” *Ann. Inst. Fourier* (Grenoble), vol. 54, no. 5, pp. 1477–1495 (2004). doi: 10.48550/arXiv.math/0307194.

[10] A. V. Faminskii, “Mixed problems for the Korteweg–de Vries equation,” *Mat. Sb.*, vol. 190, no. 6, pp. 903–935 (1999). doi: 10.1070/SM1999v190n06ABEH000408.

[11] A. V. Faminskii, “On an initial boundary value problem in a bounded domain for the generalized Korteweg–de Vries equation,” *Funct. Differ. Equ.*, vol. 8, nos. 1–2, pp. 183–194 (2001).

[12] N. A. Larkin, “Korteweg–de Vries and Kuramoto–Sivashinsky equations in bounded domains,” *J. Math. Anal. Appl.*, vol. 297, no. 1, pp. 169–185 (2004). doi: 10.1016/j.jmaa.2004.04.053.

[13] N. A. Larkin, “Korteweg–de Vries equation in bounded domains,” Bol. Soc. Paran. Mat., vol. 22, no. 1, pp. 30–37 (2004). doi: 10.5269/bspm.v22i1.7493.

[14] B. Gwaxa and S. Jamal, “First integral blow-up solutions to complex-valued KdV equations,” *J. Interdiscip. Math.*, vol. 26, pp. 747–759 (2023). doi: 10.47974/JIM-1511.

[15] N. M. Koshkarbayev and B. T. Torebek, “Nonexistence of travelling wave solution of the Korteweg–de Vries Benjamin–Bona–Mahony equation,” *Int. J. Math. Phys.*, vol. 10, no. 1, pp. 51–55 (2019). doi: 10.26577/ijmph-2019-i1-7.

[16] G. G. Doronin and N. A. Larkin, “KdV equation in domains with moving boundaries,” *J. Math. Anal. Appl.*, vol. 328, no. 1, pp. 503–517 (2007). doi: 10.1016/j.jmaa.2006.05.057.

[17] L. A. Medeiros, J. Límaco, and S. B. Menezes, “Vibrations of elastic strings: Mathematical aspects, Part One,” *J. Comput. Anal. Appl.,* vol. 4, no. 3, pp. 91–127 (2002). doi: 10.1023/A:1012934900316.

[18] L. A. Medeiros, J. Límaco, and S. B. Menezes, “Vibrations of elastic strings: Mathematical aspects, Part Two,” *J. Comput. Anal. Appl.,* vol. 4, no. 3, pp. 211–263 (2002). doi: 10.1023/A:1013151525487.

[19] J. Crank and P. Nicolson, “A practical method for numerical evaluation of solutions of partial differential equations of the heat conduction type,” *Math. Proc. Camb. Philos. Soc.,* vol. 43, no. 1, pp. 50–67 (1947). doi: 10.1017/S0305004100023197.

[20] N. J. Zabusky and M. D. Kruskal, “Interaction of ‘solitons’ in a collisionless plasma and the recurrence of initial states,” *Phys. Rev. Lett.*, vol. 15, no. 6, pp. 211–263 (1965). doi: 10.1103/PhysRevLett.15.240.

Received January, 2025